



EFFECT OF UNIT CELL HEIGHT ON THE BALLISTIC PERFORMANCE OF THE BODY-CENTERED LATTICE STRUCTURES

Oktay Kaya¹ , Hakan Hafizoğlu² , Nazim Babacan^{*1} 

¹Department of Mechanical Engineering, Faculty of Engineering and Natural Sciences, Sivas University of Science and Technology, Sivas 58140, Turkey

²TUBITAK Defense Industries Research and Development Institute, P.K. 16 06261 Mamak, Ankara, Turkey

Abstract

Original scientific paper

Lattice structures, produced by metal additive manufacturing technology, can be a potential alternative in armor applications, which are important parts of defense technologies due to their shock wave damping, energy absorption and light-weight properties. Despite the fact that the protection of metal lattice structures against explosives has been frequently investigated in the literature, their perforation performance is rarely studied. In this research, numerical ballistic penetration tests were carried out with Johnson-Cook strength and failure model parameters by using LS-DYNA software. AlSi10Mg alloy was chosen as a lattice material, which has high energy absorption ability. Both width and length were chosen as 4 mm for the body-centered lattice structure, while eight different cell height (3, 4, 5, 6, 7, 8, 9 and 15 mm) were used as unit cell parameters. The results show that the ballistic performance of lattice structures could be improved by optimizing the unit cell height for the body-centered lattice structures.

Keywords: AlSi10Mg, ballistic, energy absorption, lattice structure, LS-DYNA.

1 Introduction

Ballistic performance of the materials against rapidly penetrating objects has long been a significant research topic. Composite structures, ceramics, polymers, metal alloys such as titanium, steel, aluminum, are generally preferred in armor designs individually or in combinations. These materials have some advantages over each other according to the usage area. Low-density aluminum alloys are substantially used in the applications where the weight is a crucial design criterion. For example, it is known that 5083 aluminum alloy, which exhibits successful properties in terms of ballistic performance, is used as an armor element in the M113 personnel vehicle [1] and 2139 aluminum alloy is utilized in the CAMEL armored vehicle in a similar manner [2].

The researchers have been generally focused on the ballistic perforation performance of the plate-shaped alloys up to date [3-6]. One of the important reasons for this preference is that the production techniques used until the last decade did not allow manufacturing of complex parts. The production of alloys with a much more complex structure has become possible with the additive manufacturing method that has emerged in recent years. Unlike the traditional methods, additive manufacturing enables the production of cellular materials with complex geometries owing to its layer-based production technique. For example, open-cell structures, which are called "lattice structures", consisting of struts with a diameter of several hundred microns, can be easily produced by this technology. AlSi10Mg alloy is one of the most produced

aluminum alloys by additive manufacturing today, and it is one of the few alloys that is widely produced with selective laser melting (SLM) [7].

Among other metal additive manufacturing processes, SLM stands out with its design flexibility, short production cycle, high geometric accuracy, relatively low production costs, and ability to form suitable microstructures. Layer-wise production occurs by melting each layer with laser in a bed of metal powder in SLM. Li et al. [8] demonstrated the superiority of AlSi10Mg lattice structures manufactured by SLM in absorbing energy to a degree that reaches the level of titanium alloy lattice structures.

It has been determined that lattice structures absorb and distribute the dynamic effect quite well and that these structures can be successfully applied in passive protection systems [9]. However, so far, the number of the scientific studies related with the ballistic perforation resistance of the lattice structures is quite limited. Hassanin et al. [10] numerically compared the energy absorption capacity of the plate-shaped and auxetic lattice-structured Ni-Ti alloys and they found that energy absorption per mass of the lattice structure is approximately two times higher than that of the bulk structure. On the other hand, there is no published work on the ballistic performance of the body-centered cubic whose dynamic energy absorbing performance were substantially investigated by the researchers and found to be encouraging [11].

Besides the lattice type, factors such as cell dimensions are critical in terms of mechanical

* Corresponding author.

E-mail address: nazimbabacan@sivas.edu.tr (N. Babacan)

Received 06 January 2022; Received in revised form 22 February 2022; Accepted 21 March 2022

2587-1943 | © 2022 IJIEA. All rights reserved.

Doi: <https://doi.org/10.46460/ijiea.1054219>

performance of the lattice geometries. The variation of each parameter may cause the material to behave differently in terms of ballistic performance [12]. In this study, lattice structures with different body-centered unit cell dimensions (cubic or tetragonal) were designed in order to investigate the effects of the unit cell height on the ballistic performance. Numerical perforation tests were conducted, and the residual velocity of the projectiles were compared for the different designs. Therefore, the most protective body-centered structure among these designs in terms of the perforation resistance were revealed as a result of this study.

2 Materials and Method

The ballistic numerical simulations were done in an explicit solver of the non-linear finite element method, LS-DYNA, which is suitable for modelling ballistic problems [13]. Strength and damage evolution for ductile materials were modeled with Johnson Cook material model (MAT_15) [14]. The Eqs. (1)-(3) show the fracture criteria, damage parameters and failure damage, respectively. Johnson Cook material model have some essential properties like simulating von Mises plasticity, initial yielding, linear elasticity, strain hardening, strain-rate hardening, damage evolution and fracture [15]. The model calculates equivalent stress (σ) with using of temperature (T), strain rate ($\dot{\epsilon}$) and strain (ϵ) parameters as presented in Eq. (1):

$$\sigma(\epsilon, \dot{\epsilon}, T) = [A + B\epsilon^n] \left[1 + C \ln \frac{\dot{\epsilon}}{\dot{\epsilon}_{ref}} \right] \left[1 - \left(\frac{T - T_0}{T_m - T_0} \right)^m \right] \quad (1)$$

A , B , n parameters refer to yield stress at reference strain rate, strain hardening parameter and strain hardening exponent, respectively. While C is strain rate sensitivity, m represents the temperature exponent. T_0 , T_m are reference and melting temperatures, respectively and $\dot{\epsilon}_{ref}$ is the reference strain rate.

Fracture strain (ϵ_f) for Johnson-Cook material model is calculated with the stress triaxiality (σ^*), strain rate ($\dot{\epsilon}$) and temperature as given in Eq. (2):

$$\epsilon_f(\sigma^*, \dot{\epsilon}, T) = [D_1 + D_2 e^{D_3 \sigma^*}] [1 + D_4 \ln \dot{\epsilon}] \left[1 + D_5 \frac{T - T_0}{T_m - T_0} \right] \quad (2)$$

where $D_1 - D_5$ are empirical coefficients of the materials.

Damage evolution is zero while the material is exposed to elastic deformation. Damage evolves after some certain threshold of the accumulated plastic strain. The equation of Johnson Cook damage evolution is shown in Eq. (3) [13]:

$$\dot{D} = \begin{cases} 0, & \epsilon < p_d \\ \frac{D_c}{\epsilon_f - p_d} \dot{\epsilon}, & \epsilon \geq p_d \end{cases} \quad (3)$$

p_d is the damage threshold, ϵ_f is the fracture strain and D_c is the critical damage parameter. Solid bodies were defined with elements using nodes and meshes and every element has a damage value. If \dot{D} reaches to 1, the element is deleted and removed from simulation.

In this study, AlSi10Mg alloy produced by SLM method was used as target materials and 4340-H steel was selected as projectile material. Johnson–Cook strength and damage model parameters for AlSi10Mg [16] and 4340-H steel [17] were taken from the literature and tabulated in Table 1. Since the damage parameter was not added for steel, “EFFEPS” (maximum effective strain at failure) parameter was selected as 0.3 in the “MAT_ADD_EROSION” section of the model. Mie Grüneisen, one of Equation of State function, for AlSi10Mg were also adapted from [17] which was originally used for modelling 7075-T6 aluminum alloy. Mie Grüneisen for steel was taken from [18]. Materials were assumed be isotropic, therefore the material response is equal in all directions.

Table 1. Johnson–Cook material and damage model parameters for AlSi10Mg and steel.

Material model parameters	AlSi10Mg [10]	4340-H Steel [11]
A	167 MPa	791 MPa
B	396 MPa	510 MPa
n	0.551	0.26
C	0.001	0.014
m	0.859	1.03
D_1	0	0
D_2	0.873	0
D_3	-0.449	0
D_4	0.00147	0
D_5	0.8	0

2.1 Numerical Modeling for Verification

Verification of the material model parameters was done by simulating the experimental perforation study performed by Kristoffersen et. al. [19]. Additively manufactured AlSi10Mg plates with a dimension of 100 x 80 x 5 mm³ was exposed to AP 7.62 mm 4340-H steel bullets which was fired with initial velocities in the range of between 300 and 725 m/s. The finite element models of the projectile and the plate were presented in Figure 1.

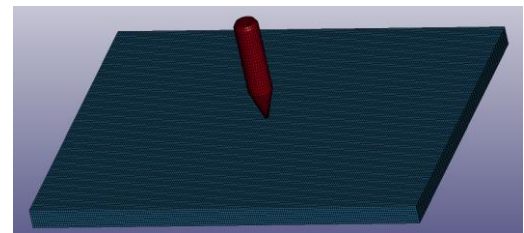


Figure 1. AP 7.62 bullet and AlSi10Mg plate numerical setup.

2.2 Modeling of the Lattice Structures

Lattice structures with body-centered unit cells were created in SolidWorks CAD system as target elements. Unit cell length and width of the designed lattice structures were chosen as 4 mm and cell heights of 3, 4, 5, 6, 7, 8, 9 and 15 mm were used to examine the effect of cell height. Therefore, cell aspect ratio which will be defined as unit cell height divided by the unit cell length or width was varied. The weight of all lattice samples was kept constant by adjusting the strut diameter of lattices. Target lattice structures were named by their unit cell dimensions. All the lattice structures were designed by

considering the total volume of $30 \times 30 \times 30 \text{ mm}^3$. Lattice material was selected as AlSi10Mg alloy. To improve the ballistic response of the lattice structures, a 2 mm AlSi10Mg plate was placed in front of the lattice structures where the first impact of the projectile occurs. Some of the modelled lattice unit cells as well as an example of entire lattice target were seen in Figure 2. A cylinder-shape 4340H steel with a diameter of 5 mm and a length of 8 mm was chosen as the projectile geometry. An initial velocity of 600 m/s was used for the projectile.

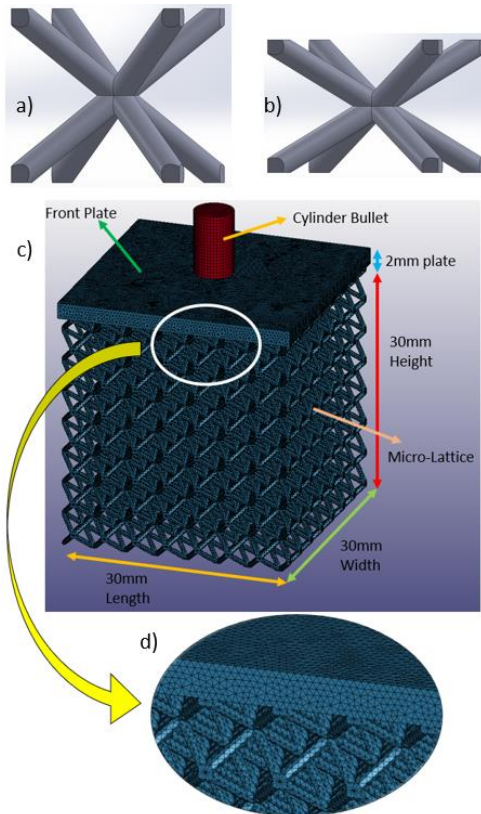


Figure 2. Geometry of the unit cells: (a) 4x4x4, (b) 4x4x3. (c) The numerical model of a target lattice structure with 4x4x4 unit cell dimensions with cylindrical projectile (d) mesh detail of the part shown with white color in (c).

Projectile was modelled with hexahedron elements, with an element size of $0.8 \times 0.8 \times 0.8 \text{ mm}^3$ whereas the lattice structure was modelled with tetrahedron elements. The maximum tetrahedron element size was chosen as 0.4 mm after conducting a mesh dependency study. Each simulation model has totally approximately one million elements. The lattices were fixed from their bottom edge faces with a boundary condition. “ERODING_SINGLE_SURFACE” eroding algorithm was used with 0.2 static friction value. Hourglass type and Hourglass coefficient parameter were chosen as 4 and 0.1, respectively.

3 Results and Discussion

3.1 Verification Study

An experimental study conducted by Kristoffersen et al. [19] was modelled to verify our numerical model. The residual velocity values of the AP7.62 bullets obtained from our numerical models were compared with the

experimental values fitted by Recht–Ipson model [19] and this comparison was shown with the calculated numerical error values in Table 2. Low numerical values verify our ballistic model including Johnson-Cook material model parameters.

Table 2. Residual velocities after perforations.

Initial Velocity (m/s)	Residual Velocity [19] (m/s)	Residual Velocity (Our Result) (m/s)	Numerical Error (%)
725	689	680	1.31
600	556	553	0.54
450	389.5	391	-0.39
300	197.8	207	4.65
200	0	0	0

3.2 Lattice Structure Study

Numerical ballistic resistance of the lattice structures with different cell heights but in same weights were performed by means of perforation tests. Residual velocity values of the projectiles which has initial velocity of 600 m/s are shown in Figure 3 as a histogram. The residual velocities were obtained in the range of 473–484 m/s. Hence, the lattice structures with front thin-plates absorbed 34.9% to 37.8% of kinetic energy of the penetrator. It is seen that the residual velocity decreased continuously when the cell height was increased from 3 to 6 mm or in other words aspect ratio of the unit cell was increased from 0.75 (3/4) to 1.5 (6/4). Then, residual velocity slightly increased with increasing cell height from 6 to 9 mm as well as in 15 mm cell length as shown in Figure 3. It should be also stated that almost same residual velocity (477 m/s) was obtained for the 10 mm and 12 mm samples which were not included in the Figure 3. While the maximum residual velocity is at 4x4x3 geometry with 484 m/s, the minimum residual velocity was found at 4x4x6 geometry with 473 m/s. Even if the residual velocity difference seen in the different lattice structures seems to be relatively low, just modifying the one geometric parameter of the unit cell without changing the mass could lead to obtain more efficient lattice armor structure. The results also indicated that 6 mm cell height which corresponds to aspect ratio of 1.5 is the turning point of the deformation behavior for 4-mm body-centered structures. In addition, increasing the aspect ratio above value of 2 did not influence the ballistic behavior of the lattice structures prominently.

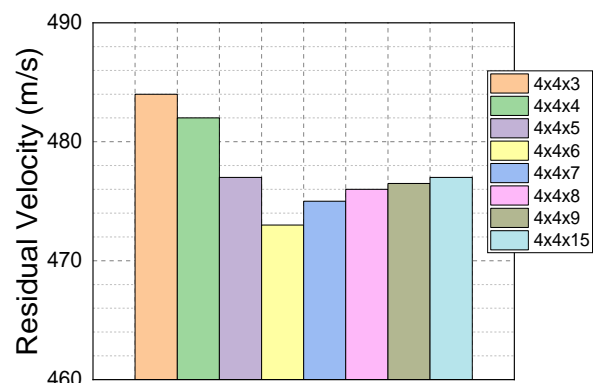


Figure 3. Residual velocities of the projectiles with initial velocity of 600 m/s after perforating the different lattice structures.

Section views of the 4x4x4 lattice structure and the projectile was presented in Figure 4 to illustrate the deformation behavior of the both structures during the penetration. The first interaction of the projectile on the lattice structure caused to a densification as seen in Figure 4 (a). The layers of the lattice structure tried to resist against to the projectile by getting closer as explained in the study of Hassanin [10] for the auxetic structures. It is also seen that AlSi10Mg target was deformed locally and the material has been subjected to local fractures in Figure 4 (b). As expected, there was not much deformation on the steel projectile, which is much harder than aluminum. It should be noted that deformation of the only one of the lattice structures was presented since there is no visible discrepancy between the deformation behavior of the different lattice structures.

Bai et al. [20] found that additively manufactured Ti-6Al-4V body-centered lattice structures with small aspect ratio have larger energy absorption capacity compared to those have larger aspect ratio as a result of the quasi-static tests. They attributed this result to the failure mode of the structures by changing the aspect ratio and they observed that lattice structure with a larger aspect ratio has more cracks, unlike to the counterparts which showed more stable mechanical response. However, an opposite trend was seen in this study for cell height in the 3-6 mm range and lattice structures with large aspect ratio absorbed more energy. This could be sourced from the difference of the deformation behavior of AlSi10Mg alloys than Ti-6Al-4V structures, as well as the difference of the dynamical response from the static response.

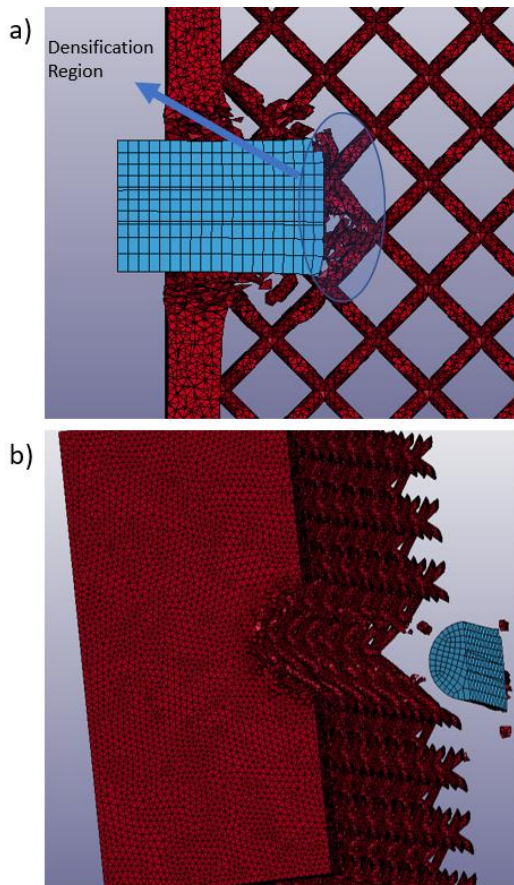


Figure 4 The deformation of 4x4x4 lattice structure: a) during the first transition of the projectile from the front plate to the lattice structure b) after perforation.

The velocity change of the projectiles which penetrate three different lattice structures were shown in Figure 5 as a function of time. An initial rapid decline in the velocity for all the models takes place until the projectile passes the front plate. Afterwards, a further decrease in velocity but with lower slopes which corresponds to the interaction of the bullet with the lattice structure is observed for all numerical analyses. While the slopes of the velocity drop of the 4x4x6 and 4x4x15 are almost equal, it is lower for the 4x4x3 lattice structure. This stage shows the more successful performance of the 4x4x6 and 4x4x15 structures in terms of the ballistic performance. Moreover, it is observed that the penetrator completely pierced the lattice structures in approximately 80 μs for all the numerical tests.

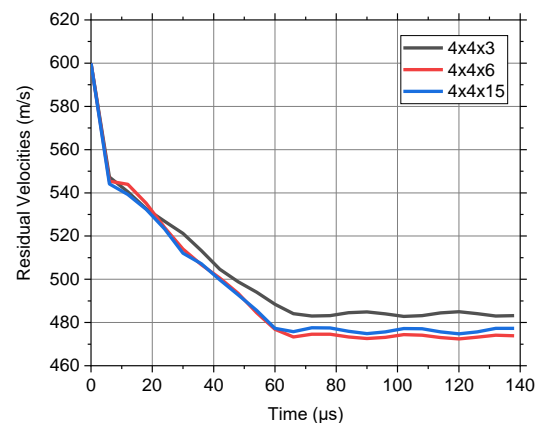


Figure 5 Residual velocities of 4x4x3, 4x4x6 and 4x4x15 lattice structures with respect to time.

4 Conclusion

In this study, ballistic performance of body-centered lattice structures which have different cell heights was investigated. Resistance against the penetration was improved by increasing the aspect ratio of the unit cell from 0.75 to 1.5. A further increase resulted in a decrease in ballistic performance. The minimum and maximum residual velocities were obtained at 4x4x6 and 4x4x3 lattice structures, respectively. The energy absorption difference of these structures was found to be approximately 8.3 %. The results show that the ballistic performance of lattice structures can be improved by optimizing the unit cell height parameter. Further research related to the effect of lattice geometry on the experimental ballistic performance is still under development.

Declaration

This study does not require ethics committee approval.

References

[1] Constellium awarded contract with TARDEC, the US army tank automotive research development and engineering center. *Constellium*. Retrieved November 30, 2018 from <https://www.constellium.com/news/2016/09/28/constellium-awarded-contract-tardec-us-army-tank-automotive-research-development-and>

- [2] Balos, S., Howard, D., Brezulianu, A., & Labus Zlatanović, D. (2021). Perforated plate for ballistic protection—A review. *Metals*, 11(4), 526.
- [3] Luo, D., Wang, Y., Wang, F., Cheng, H., Zhang, B., & Zhu, Y. (2020). The influence of metal cover plates on ballistic performance of silicon carbide subjected to large-scale tungsten projectile. *Materials & Design*, 191, 108659.
- [4] Flores-Johnson, E., Saleh, M., & Edwards, L. (2011). Ballistic performance of multi-layered metallic plates impacted by a 7.62-mm APM2 projectile. *International Journal of Impact Engineering*, 38(12), 1022-1032.
- [5] Yunfei, D., Wei, Z., Yonggang, Y., & Gang, W. (2014). The ballistic performance of metal plates subjected to impact by projectiles of different strength. *Materials & Design*, 58, 305-315.
- [6] Zhang, R., Qiang, L., Han, B., Zhao, Z., Zhang, Q., Ni, C., & Lu, T. J. (2020). Ballistic performance of UHMWPE laminated plates and UHMWPE encapsulated aluminum structures: Numerical simulation. *Composite Structures*, 252, 112686.
- [7] Laurençon, M., De Rességuier, T., Loison, D., Baillargeat, J., Ngnekou, J. D., & Nadot, Y. (2019). Effects of additive manufacturing on the dynamic response of AlSi10Mg to laser shock loading. *Materials Science and Engineering: A*, 748, 407-417.
- [8] Liu, X., Sekizawa, K., Suzuki, A., Takata, N., Kobashi, M., & Yamada, T. (2020). Compressive properties of Al-Si alloy lattice structures with three different unit cells fabricated via laser powder bed fusion. *Materials*, 13(13), 2902.
- [9] Płatek, P., Sienkiewicz, J., Janiszewski, J., & Jiang, F. (2020). Investigations on mechanical properties of lattice structures with different values of relative density made from 316L by selective laser melting (SLM). *Materials*, 13(9), 2204.
- [10] Hassanin, H., Abena, A., Elsayed, M. A., Essa, K. (2020). 4D Printing of NiTi Auxetic Structure with Improved Ballistic Performance, *Micromachines*, 11(8), 745.
- [11] Sadeghi, H., Bhate, D., Abraham, J., & Magallanes, J. (2018). Quasi-static and dynamic behavior of additively manufactured metallic lattice cylinders. *AIP Conference Proceedings*, 1979, 070029
- [12] Tancogne-Dejean, T., Spierings, A. B., & Mohr, D. (2016). Additively-manufactured metallic micro-lattice materials for high specific energy absorption under static and dynamic loading. *Acta Materialia*, 116, 14-28.
- [13] Hafizoglu, H., Durlu, N., & Konokman, H. E. (2019). Effects of sintering temperature and Ni/Fe ratio on ballistic performance of tungsten heavy alloy fragments. *International Journal of Refractory Metals and Hard Materials*, 81, 155-166.
- [14] Børvik, T., Hopperstad, O. S., & Pedersen, K. O. (2010). Quasi-brittle fracture during structural impact of AA7075-T651 aluminium plates. *International Journal of Impact Engineering*, 37(5), 537-551.
- [15] LS-Dyna Keyword User's Manual, vol. I. (2007). *Livermore Software Technology Corp.* Retrieved July 29, 2021 from https://www.lstc.com/pdf/ls-dyna_971_manual_k.pdf
- [16] Segebade, E., Gerstenmeyer, M., Dietrich, S., Zanger, F., & Schulze, V. (2019). Influence of anisotropy of additively manufactured AlSi10Mg parts on chip formation during orthogonal cutting. *Procedia CIRP*, 82, 113-118.
- [17] Fras, T., Colard, L., & Pawlowski, P. (2015). Perforation of aluminum plates by fragment simulating projectiles (FSP). *The International Journal of Multiphysics*, 9(3), 267-286.
- [18] Elshenawy, T., & Li, Q. (2013). Influences of target strength and confinement on the penetration depth of an oil well perforator. *International Journal of Impact Engineering*, 54, 130-137.
- [19] Kristoffersen, M., Costas, M., Koenis, T., Brøtan, V., Paulsen, C. O., & Børvik, T. (2020). On the ballistic perforation resistance of additive manufactured AlSi10Mg aluminium plates. *International Journal of Impact Engineering*, 137, 103476.
- [20] Bai, L., Gong, C., Chen, X., Zheng, J., Yang, J., Li, K., & Sun, Y. (2021). Heterogeneous compressive responses of additively manufactured Ti-6Al-4V lattice structures by varying geometric parameters of cells. *International Journal of Mechanical Sciences*, 214, 106922.